In Situ XRD Observation of Crystal Deformation of Piezoelectric (K,Na)NbO3 Thin Films

Tan, Goon
Hyo Kweon, Sang
Shibata, Kenji
Yamada, Tomoaki
Kanno, Isaku

(Citation)
ACS Applied Electronic Materials,2020(2):2084-2089

(Issue Date)
2020-07-06

(Resource Type)
journal article

(Version)
Accepted Manuscript

In situ XRD Observation of Crystal Deformation of Piezoelectric (K,Na)NbO_3 Thin Films

Goon Tan[†]*, Sang Hyo Kweon*[†]*, Kenji Shibata*[‡]*, Tomoaki Yamada*[⊥,§]*, and Isaku Kanno*[*,†]

[†]Mechanical Engineering, Kobe University, 1-1 Rokkodai-cho, Nada-ku, Kobe 657-8501, Japan

[‡]SCIOCS, 880, Isagozawa-cho, Hitachi-shi, Ibaraki-ken 319-1418, Japan

[⊥]Department of Energy Engineering, Nagoya University, Furo-cho, Chikusa-ku, Nagoya 464-8603, Japan

[§]PRESTO, Japan Science and Technology Agency, Kawaguchi 332-0012, Japan

* To whom correspondence should be addressed

Email: kanno@mech.kobe-u.ac.jp

KEYWORDS: *in situ* XRD measurements, lead-free KNN thin films, crystallographic deformation, crystal phase transition, piezoelectric properties

ABSTRACT

$(K,Na)NbO_3$ (KNN) thin films are promising lead-free piezoelectric materials for microelectromechanical systems (MEMS) devices. However, the origin of the strong piezoelectric properties of KNN thin films remains unclear because crystallographic deformation by piezoelectric effects is not clear in detail. We used synchrotron X-ray diffraction (XRD) to explore the origin of the piezoelectricity of polycrystalline $(K_{0.45}Na_{0.55})NbO_3$ (KNN) thin films which led to the observation of large crystal deformation originating from the piezoelectric effects. The peak shifts of the XRD patterns indicated changes in both the out-of-plane and in-plane lattice parameters of KNN. In addition, an electric-field-induced phase transition under an applied electric field was observed. The microscopic piezoelectric coefficients ($e_{31,f}$) were estimated from the *in situ* XRD results and subsequently compared with the macroscopic piezoelectric coefficients estimated from the converse piezoelectric effect by the cantilever method. The macroscopic $|e_{31,f}|$ coefficients based on the converse piezoelectric effect were in the range 6.3–11.1 C/m^2, whereas the microscopic $|e_{31,f}|$ values based on the *in situ* XRD results were in the range 1.2–1.5 C/m^2. However, the macroscopic piezoelectric coefficients from the direct piezoelectric effect were 1.6–2.0 C/m^2, which were similar to those obtained from the *in situ* XRD results. The results suggest that the large macroscopic piezoelectric properties associated with the converse piezoelectric effect arise from the observed electric-field-induced phase transition. This study demonstrates the main factors associated with the macroscopic piezoelectric properties in lead-free KNN thin films.

1. INTRODUCTION

Piezoelectric thin films have been widely investigated for their potential applications in various microelectromechanical systems (MEMS) such as microsensors and microactuators.[1–5] Among various piezoelectric thin-film materials, lead zirconate titanate $Pb(Zr,Ti)O_3$ (PZT) is the most popular for piezoelectric MEMS because of its superior piezoelectric properties.[6,7] However, environmental concerns persist because PZT-based piezoelectric materials contain toxic lead. Therefore, efforts to mitigate the environmental impact of piezoelectric devices that contain lead-based piezoelectric materials have led to the development of lead-free piezoelectric materials. Several candidates for lead-free piezoelectric materials have been investigated for use in thin-film devices, including $BiFeO_3$ (BFO),[8–10] AlN,[11–13] and $(K,Na)NbO_3$ (KNN).[14–17] Among these materials, KNN is the most promising because of its high Curie temperature and good piezoelectric properties. Numerous researchers have reported that KNN thin films exhibit strong piezoelectric properties, and piezoelectric energy harvesters with KNN thin films have an output power comparable to that of harvesters with PZT thin films.[17,18] However, the origin of the strong piezoelectric properties of KNN thin films remains unclear because crystallographic deformation by piezoelectric effects is not yet understood in detail. Recent progress with *in situ* X-ray diffraction (XRD) measurements has enabled us to observe directly how the crystal structures of ferroelectric thin films change under an applied electric field.[19–23] In a previous study, we reported a comparative investigation of the macroscopic and microscopic piezoelectric properties of PZT thin films using two approaches: the cantilever method and *in situ* XRD measurements.[24] We found that the piezoelectric property of a polycrystalline PZT thin film is larger than that of an epitaxial PZT thin film, likely because of a rotation of the polarization direction accompanied by a crystal phase transition or domain reorientation in the polycrystalline PZT thin film.

In the present study, we performed *in situ* XRD measurements of polycrystalline KNN thin films on Si substrates under an applied DC bias voltage to clarify the origin of the relatively large piezoelectricity of KNN thin films. We also evaluated the transverse piezoelectric properties using the cantilever method,[25–27] whereupon we conducted a comparative study of the macroscopic and microscopic piezoelectric properties of KNN thin films. To further enhance the piezoelectric properties of KNN thin films, it is important to understand how crystal deformation contributes to their macroscopic piezoelectric properties.

2. EXPERIMENTAL SECTION

KNN thin films with a K/Na ratio of 45/55 were prepared on (111)/Pt/Ti/SiO_2/Si substrates by radio frequency magnetron sputtering. The detailed deposition conditions have been described elsewhere.[17] The film thickness was 2 μm. Before the *in situ* XRD measurements, we confirmed the crystal structures by conventional XRD using a four-axis diffractometer with Cu Kα radiation source (Rigaku, SmartLab). The films exhibited a polycrystalline and perovskite structure with a preferential (001) orientation in the out-of-plane direction (see Figure S1, Supporting Information), as reported previously.[15,17] The samples were cut into rectangular cantilever beams to determine the transverse piezoelectric coefficients ($e_{31,f}$) by the cantilever method, which we used to evaluate both the direct and converse piezoelectric effects. The converse piezoelectric coefficient was determined by measuring the cantilever displacement induced by an applied electric field. We applied a negative unipolar sinusoidal voltage to the top electrode at a frequency of 600 Hz, which was sufficiently lower than the resonance frequency. We calculated the direct piezoelectric coefficient by measuring the charge generated from the tip displacement of the cantilever. Here we used a precise actuator to apply a periodic input displacement (5–20 μm) at a frequency of 20 Hz to the free end of the cantilever. The details of the cantilever method via the direct and

converse piezoelectric effects are described elsewhere.[27] The room-temperature ferroelectric hysteresis loops of the KNN thin films were recorded by a Precision Multiferroic II ferroelectric tester (Radiant Technologies, Inc.). The *in situ* XRD experiments were conducted using synchrotron radiation with a 12.4 keV photon energy (λ = 0.1 nm) on the BL19B2 and BL46XU beamlines at the SPring-8 synchrotron research facility in Japan. We measured the same cantilever samples in the *in situ* XRD experiments. The KNN cantilever specimen was fixed to the stage by a double-sided tape. The top and bottom electrodes of the KNN specimen were connected to a power generator by Au wires, and a DC power source was used to provide a stable bias field. We first applied -5 V (-25 kV/cm), which was higher than the coersive electric field of the KNN thin film as a poling treatment. All the measurements were carried out at room temperature. Details of the setup for the *in situ* XRD measurements have been described in an earlier report.[24]

3. RESULTS AND DISCUSSION

3.1. *In situ* XRD Observation of KNN Thin Films

Figure 1a shows the out-of-plane XRD θ–2θ patterns around KNN *004* under a negative DC voltage. Our previous paper demonstrated that polycrystalline KNN thin films deposited onto Pt/Ti/SiO_2/Si substrates exhibit pseudo-cubic or tetragonal perovskite structures.[15–17] In general, the bulk KNN in this composition (K/Na=45/55) shows orthorhombic or monoclinic phase.[28] According to our previous paper,[15,29] the crystal structures of KNN thin films were considered to be tetragonal or pseudo-cubic, which seemed different from those of bulk ceramics. This difference might be due to the constraints from substrates. According to the present XRD patterns obtained using synchrotron radiation, pseudo-cubic and tetragonal phases appear to coexist in the KNN thin film, as shown in Figure 1b. Considering the peak positions and intensities of two split KNN peaks between out-of-plane and in-plane XRD discussed later, we indexed the split two peaks as pseudo-cubic and tetragonal phases. We used the Gaussian function (Igor Pro 8.04) to conduct the peak

fitting and the peak separation. The values in lattice parameters of pseudo-cubic and tetragonal KNN crystals were found to be similar to those of cubic and tetragonal phases reported in the previous paper about Rietveld analysis of bulk KNN.[30] We confirmed that the KNN *004* peak shifted to a lower angle with increasing magnitude of the applied voltage. We also found that the electrode Pt *111* peak remained unchanged (see Figure S2, Supporting Information). Therefore, the observed KNN peak shifts were due to the deformation of the KNN crystal lattice originating from the converse piezoelectric effect. It was found that with increasing voltage, the proportion of the tetragonal phase increased, whereas that of the pseudo-cubic phase decreased, as shown in Figure 1c. We also observed the peak shifts of KNN *004* with positive DC voltages (5 V–20 V) as shown in Figure S3 (Supporting Information).

Figure 2a shows how the lattice parameter varied with the electric field, as described by the polarization–electric field (*P–E*) hysteresis loops measured at 10 Hz. The lattice parameter was estimated from the position of pseudo-cubic peak (Figure 1). When we increased the positive DC voltage from 5 V to 10 V, the lattice parameter stretched again. This reverse dependence originates from the rotation of polarization direction at an electric field larger than a coercive field, known as polarization reversal. We confirmed that the polarization-reversal characteristic compatible with the *P–E* hysteresis loops. The change in lattice parameter of tetragonal phase also exhibited similar electric field dependence, as seen in Figure S4 (Supporting Information).

We next evaluated the crystal phase variation for each external electric field from the fitting curves. We estimated the tetragonal phase ratio from the peak areas of the pseudo-cubic and tetragonal diffraction peaks, specifically, $A(004)_{\text{tetragonal}}/\{A(004)_{\text{tetragonal}} + A(004)_{\text{pseudo-cubic}}\}$.[21,31] Figure 2b shows the change of the tetragonal phase ratio as the applied electric field is varied, revealing an electric-field-induced phase transition from the pseudo-cubic phase to the tetragonal

phase. After the first cycle of negative voltages, the tetragonal phase ratio did not return to its initial value. However, when a positive voltage of 5 V was applied, the phase ratio returned to the initial state. For higher positive voltages, the tetragonal phase ratio increased again because of the polarization-reversal behavior, in agreement with the variation of the lattice parameter (Figure 2a). The maximum change in phase transition was approximately 29%. Such a transition between two phases has been reported previously in a polycrystalline PZT thin film.[32] There is also a possibility that the pseudo-cubic phase might consist of some mixture of several phases such as monoclinic and orthorhombic phases. Therefore, we are considering Rietveld analysis of our KNN films by making powders from removing substrates in the further investigation.[33]

We next performed X-ray rocking-curve measurements under applied voltages. Figure 3a shows the rocking curves of KNN *004* at voltages of 0 V, −10 V, and −20 V. The peak intensity increased and the peak width decreased with increasingly negative applied voltage. The corresponding full-width at half-maximum (FWHM) variation of the rocking curve is plotted as a function of the applied voltage in Figure 3b. The FWHM value of the rocking curve decreased with increasing applied electric field. The rocking curve contains both pseudo-cubic and tetragonal phases. The decrease of FWHM of the rocking curve indicates the enhancement of crystal orientation. We suggest that this enhancement originated from the increase of tetragonal phase as a result of the phase transition from pseudo-cubic to tetragonal phase.

Figure 4a shows the in-plane XRD measurements around the KNN *400* peak under a negative applied voltage. Notably, when a voltage of −20 V was applied, a shoulder peak was clearly observed. Figure 4b and Figure 4c show the peak profile fittings of the KNN patterns without and with a −20 V. Although the in-plane diffraction of the tetragonal phase was very weak, is was confirmed that the tetragonal phase increased with increasing DC voltage, consistent with the out-

of-plane results. Figure 4d shows the variation of the in-plane crystal lattice parameter of pseudo-cubic phase normal to the direction of the applied voltage. The in-plane crystal lattice parameter decreased linearly with increasing voltage and returned to the initial lattice parameter at −20 V. This in-plane lattice relaxation was likely caused by the large extrinsic change of the phase structure from pseudo-cubic to tetragonal, as evident in Figure 4a. When we returned the voltage, the lattice parameter became slightly larger than that at the initial state, as evident in Figure 4d. We also found the tetragonal phase ratio did not return to its original value. Notably, the measurement period of in-plane XRD was longer than that of out-of-plane XRD. Therefore, the KNN thin film was subjected to a longer DC bias for the in-plane measurements. This irreversible change in the lattice parameter and phase ratio might be due to the extended DC bias duration during the in-plane XRD measurements. We also measured the in-plane KNN *200* peaks and confirmed the similar voltage dependency. The change in in-plane lattice parameter estimated from the KNN *200* peaks was similar to that shown in Figure 4d. We estimated the Poisson's ratio from the out-of-plane strain (Figure 2a) and the in-plane strain (the linear change part in Figure 4d). Besides the low voltage of -5 V, we found that the Poisson's ratio values showed about 0.30 corresponding well to the reported value of 0.27 in KNN bulk.[34] It was suggested that there was a small deformation of the sample fixed on the stage. However, the KNN crystals may still receive some constraints from substrates. In order to measure the precise in-plane strain, we are considering the in-situ XRD measurements of free-standing films fabricated by etching process in the future investigation.[35]

3.2. Characterization of Macroscopic Piezoelectric Properties

We next compared the transverse piezoelectric properties by evaluating the electric-field-induced strain determining from the *in situ* XRD measurements and the cantilever method. The macroscopic in-plane strain component of the KNN thin film along the cantilever was estimated

on the basis of tip displacement. The macroscopic transverse piezoelectric coefficients by the converse piezoelectric effect (converse $e_{31,f}$) were obtained from the macroscopic in-plane strain measured using the cantilever method.[27] For comparison with the macroscopic $|e_{31,f}|$ coefficients, the microscopic $|e_{31,f}|$ coefficients were estimated from the *in situ* in-plane XRD measurements. The piezoelectric coefficients $d_{31,f}$ were first obtained from the relationship between the electric-field-induced strain of the in-plane direction and the electric field using $\Delta x = d_{31,f} \times E$. The intrinsic strain derived from the linear part of the change in lattice parameter (Figure 4b) was used for the calculation of $d_{31,f}$. The $d_{31,f}$ constants were around 20 pm/V. The $d_{31,f}$ constants were then converted into $e_{31,f}$ constants by multiplying the reported Young's modulus of KNN films (i.e., 67 GPa).[36] Figure 5a shows absolute values of the converse piezoelectric coefficients ($|e_{31,f}|$) estimated from the *in situ* XRD measurements and those estimated from the cantilever method. Here, we measured the macroscopic converse $|e_{31,f}|$ coefficients from -2.5 to -75 kV/cm by the cantilever method. Below -2.5 kV/cm, it was difficult to measure precisely due to a large noise. The increase of macroscopic $|e_{31,f}|$ coefficients implied large extrinsic effects.[27] The macroscopic $|e_{31,f}|$ coefficients increased gradually and became constant (6.3–11.1 C/m^2), whereas the microscopic $|e_{31,f}|$ coefficients were almost constant (1.2–1.5 C/m^2) against the electric field. The macroscopic converse $|e_{31,f}|$ coefficients were several times greater than the microscopic $|e_{31,f}|$ coefficients estimated from the *in situ* XRD measurements. The converse piezoelectric coefficients of XRD were calculated from the intrinsic lattice deformation (KNN peak shifts). The effects of crystal transition and reorientation were not included in the converse piezoelectric coefficients of XRD. On the other hand, both intrinsic and extrinsic contributions were involved in the converse piezoelectric coefficients measured by the cantilever method. It is suggested that if we can measure the converse $|e_{31,f}|$ coefficients at enough low electric field, we can get values comparable to the

$|e_{31,f}|$ coefficients measured by in situ XRD measurements. However, below -2.5 kV/cm, it was difficult to measure precisely due to a large noise. For a better discussion, we then investigated the piezoelectric coefficients from the direct piezoelectric effect (direct $e_{31,f}$) by measuring the generated charge from the periodic input displacement of the cantilever tip.[27] Notably, the direct $|e_{31,f}|$ coefficient here can be regarded as the intrinsic contribution of the lattice deformation almost without the electric field-induced extrinsic contributions. Figure 5b shows the direct $|e_{31,f}|$ coefficients as a function of the input tip displacement of the cantilever. The value of the direct $|e_{31,f}|$ coefficients was in the range 1.6–2.0 C/m^2, which is similar to the value of microscopic $|e_{31,f}|$ coefficients evaluated from the in-plane XRD peak shifts (Figure 5a). This similarity confirms the microscopic $|e_{31,f}|$ coefficients stemmed from the intrinsic lattice deformation. However, the converse $|e_{31,f}|$ coefficients measured by the macroscopic cantilever method include both intrinsic and extrinsic contributions. This result implies our polycrystalline KNN thin films contain large extrinsic contributions. In our previous paper, we found the large converse piezoelectric property of polycrystalline PZT thin films was attributed to the extrinsic piezoelectric effects.[27] The present study also demonstrated the KNN thin films showed the similar large extrinsic piezoelectric effects. In this study, we suggested the main extrinsic contributions originated from the crystal phase transition and crystal reorientation. Particularly, Figure 2b reveals a large change of 29% in the phase transition between pseudo-cubic and tetragonal phases. According to our previous paper,[24] the converse $|e_{31,f}|$ coefficients of a polycrystalline PZT thin film was larger than that of an epitaxial PZT thin film. We infer that the enhanced macroscopic piezoelectric property of the polycrystalline PZT thin film is attributed to the easy rotation of the polarization direction. Jo *et al*. investigated *in situ* XRD of polycrystalline $(Bi_{1/2}Na_{1/2})TiO_3$-$BaTiO_3$ piezoceramics.[37] They also demonstrated phase transitions caused by polarization rotation

may play an important role in maximizing properties. In this study, the observed phase transition and crystal reorientation might also be associated with polarization rotation. We consider the polarization rotation via electric field is an important factor that can greatly enhance the macroscopic piezoelectric response by the converse piezoelectric effect.

4. CONCLUSION

In summary, we demonstrated the origin of the large piezoelectric properties of KNN thin films. The *in situ* XRD measurements showed direct observation of both out-of-plane and in-plane KNN lattice deformation as well as the change in the phase transition between pseudo-cubic and tetragonal phases. According to the comparative discussion, the enhancement of piezoelectric properties evaluated by the cantilever are mostly considered to be caused by the extrinsic contributions of the phase transition (maximum ~29% variation) and crystal reorientation. The extrinsic contributions can enlarge the macroscopic piezoelectric properties more than six-fold. This study demonstrated that the extrinsic contribution is a key to improving the macroscopic piezoelectric properties of lead-free KNN thin films.

ASSOCIATED CONTENT

Supporting Information.

XRD wide scans of KNN thin films, Extra data of *in situ* XRD measurements, Out-of-plane lattice parameter including tetragonal phase as a function of applied voltage.

AUTHOR INFORMATION

Corresponding Author

* To whom correspondence should be addressed

Email: kanno@mech.kobe-u.ac.jp

Funding Sources

This study was supported by JST-CREST (grant no. JPMJCR20Q2).

Notes

The authors declare no completing financial interest.

ACKNOWLEDGMENT

The measurements were performed using the BL19B2 and BL46XU beamlines at SPring-8 and were supported by the Japan Synchrotron Radiation Research Institute (proposal nos. 2017B1604 and 2018A1562). This study was also supported by JST-CREST (grant no. JPMJCR16Q4).

REFERENCES

(1) Defaÿ, E.; Millon, C.; Malhaire, C.; Barbier, D. PZT Thin Films Integration for the Realisation of a High Sensitivity Pressure Microsensor Based on a Vibrating Membrane. *Sensors Actuators, A Phys.* **2002**, *99* (1–2), 64–67.

(2) Muralt, P.; Polcawich, R. G.; Trolier-McKinstry, S. Piezoelectric Thin Films for Sensors , Actuators , and Energy Harvesting. *MRS Bull.* **2009**, *34*, 658–664.

(3) Funakubo, H.; Dekkers, M.; Sambri, A.; Gariglio, S.; Shklyarevskiy, I.; Rijnders, G. Epitaxial PZT Films for MEMS Printing Applications. *MRS Bull.* **2012**, *37* (11), 1030–1038.

(4) Hida, H.; Morita, Y.; Kurokawa, F.; Tsujiura, Y.; Kanno, I. Simple Millimeter-Scale Robot Using Pb(Zr, Ti)O_3 Piezoelectric Thin Film Actuator on Titanium Substrate. *Microsyst. Technol.* **2016**, *22* (6), 1429–1436.

(5) Kim, S. G.; Priya, S.; Kanno, I. Piezoelectric MEMS for Energy Harvesting. *MRS Bull.* **2012**, *37* (11), 1039–1050.

(6) Jaffe, B.; Roth, R. S.; Marzullo, S. "Piezoelectric Properties of Lead Zirconate Titanate Solid-Solution Ceramics." *J. Appl. Phys.* **1954**, *25* (1954), 809–810.

(7) Kanno, I.; Fujii, S.; Kamada, T.; Takayama, R. Piezoelectric Properties of *c*-axis Oriented Pb(Zr,Ti)O_3 Thin Films. *Appl. Phys. Lett.* **1997**, *70* (11), 1378–1380.

(8) Ujimoto, K.; Yoshimura, T.; Ashida, A.; Fujimura, N. Direct Piezoelectric Properties of (100) and (111) $BiFeO_3$ Epitaxial Thin Films. *Appl. Phys. Lett.* **2012**, *100* (102901), 3–6.

(9) Ujimoto, K.; Yoshimura, T.; Wakazono, K.; Ashida, A.; Fujimura, N. Crystal Structure and Local Piezoelectric Properties of Strain-Controlled (001) $BiFeO_3$ Epitaxial Thin Films. *Thin Solid Films* **2014**, *550*, 738–741.

(10) Shimizu, K.; Hojo, H.; Ikuhara, Y.; Azuma, M. Enhanced Piezoelectric Response Due to Polarization Rotation in Cobalt-Substituted $BiFeO_3$ Epitaxial Thin Films. *Adv. Mater.* **2016**, *28*, 8639–8644.

(11) Akiyama, B. M.; Kamohara, T.; Kano, K.; Teshigahara, A.; Takeuchi, Y.; Kawahara, N. Enhancement of Piezoelectric Response in Scandium Aluminum Nitride Alloy Thin Films Prepared by Dual Reactive Cosputtering. *Adv. Mater.* **2009**, *21*, 593–596.

(12) Uehara, M.; Shigemoto, H.; Fujio, Y.; Nagase, T.; Aida, Y.; Umeda, K. Giant Increase in Piezoelectric Coefficient of AlN by Mg-Nb Simultaneous Addition and Multiple Chemical States of Nb Giant Increase in Piezoelectric Coefficient of AlN by Mg-Nb Simultaneous Addition and Multiple Chemical States of Nb. *Appl. Phys. Lett.* **2017**, *111*, 112901.

(13) Anggraini, S. A.; Uehara, M.; Yamada, H.; Akiyama, M. Scripta Materialia Mg and Ti Codoping Effect on the Piezoelectric Response of Aluminum Nitride Thin Films. *Scr. Mater.* **2019**, *159*, 9–12.

(14) Saito, Y.; Takao, H.; Tani, T.; Nonoyama, T.; Takatori, K.; Homma, T.; Nagaya, T.; Nakamura, M. Lead-Free Piezoceramics. *Nature* **2004**, *432*, 84–87.

(15) Shibata, K.; Oka, F.; Nomoto, A.; Mishima, T.; Kanno, I. Crystalline Structure of Highly Piezoelectric (K, Na)NbO_3 Films Deposited by RF Magnetron Sputtering Crystalline Structure of Highly Piezoelectric (K, Na)NbO_3 Films Deposited by RF Magnetron Sputtering. *Jpn. J. Appl. Phys.* **2008**, *47* (12), 8909–8913.

(16) Shibata, K.; Oka, F.; Ohishi, A.; Mishima, T.; Kanno, I. Piezoelectric Properties of (K,Na)NbO_3 Films Deposited by RF Magnetron Sputtering. *Appl. Phys. Express* **2008**, *1* (011501), 1–3.

(17) Shibata, K.; Suenaga, K.; Watanabe, K.; Horikiri, F. Improvement of Piezoelectric Properties of (K, Na)NbO_3 Films Deposited by Sputtering. *Jpn. J. Appl. Phys.* **2011**, *50*, 041503.

(18) Kanno, I.; Ichida, T.; Adachi, K.; Kotera, H.; Shibata, K. Sensors and Actuators A : Physical Power-Generation Performance of Lead-Free (K, Na)NbO_3 Piezoelectric Thin-Film Energy Harvesters. *Sensors Actuators A. Phys.* **2012**, *179*, 132–136.

(19) Fujisawa, T.; Ehara, Y.; Yasui, S.; Kamo, T.; Yamada, T.; Sakata, O.; Funakubo, H. Direct Observation of Intrinsic Piezoelectricity of Pb(Zr,Ti)O_3 by Time-Resolved X-Ray Diffraction Measurement Using Single-Crystalline Films. *Appl. Phys. Lett.* **2014**, *105* (1), 012905.

(20) Sato, T.; Ichinose, D.; Oshima, N.; Mimura, T.; Nemoto, Y.; Shimizu, T.; Imai, Y.; Uchida, H.; Sakata, O.; Funakubo, H. Time Response Demonstration of in Situ Lattice Deformation under an Applied Electric Field by Synchrotron-Based Time-Resolved X-Ray Diffraction in Polar-Axis-Oriented Epitaxial Pb (Zr, Ti)O_3 Film. *Jpn. J. Appl. Phys.* **2018**, *57* (0902B8), 1–5.

(21) Nakajima, M.; Wada, A.; Yamada, T.; Ehara, Y.; Kobayashi, T.; Funakubo, H. Impact of Pulse Poling on Static and Dynamic Ferroelastic-Domain Contributions in Tetragonal Pb(Ti, Zr)O_3 films Determined by in-Situ x-Ray Diffraction Analysis. *J. Appl. Phys.* **2014**, *116*, 194102.

(22) Lee, K. S.; Yong Kwan Kim; Baik, S.; Kim, J.; II Sub Jung. In Situ Observation of Ferroelectric 90°-Domain Switching in Epitaxial Pb(Zr, Ti)O_3 Thin Films by Synchrotron X-Ray Diffraction. *Appl. Phys. Lett.* **2001**, *79*, 2444–2446.

(23) Davydok, A.; Cornelius, T. W.; Mocuta, C.; Lima, E. C.; Araujo, E. B.; Thomas, O. In Situ X-Ray Diffraction Studies on the Piezoelectric Response of PZT Thin Films. *Thin Solid Films* **2016**, *603*, 29–33.

(24) Tan, G.; Maruyama, K.; Kanamitsu, Y.; Nishioka, S.; Ozaki, T.; Umegaki, T.; Hida, H.; Kanno, I. Crystallographic Contributions to Piezoelectric Properties in PZT Thin Films. *Sci. Rep.* **2019**, *9*, 7309.

(25) Kanno, I.; Kotera, H.; Wasa, K. Measurement of Transverse Piezoelectric Properties of PZT Thin Films. *Sensors Actuators, A Phys.* **2003**, *107* (1), 68–74.

(26) Chun, D. M.; Sato, M.; Kanno, I. Precise Measurement of the Transverse Piezoelectric Coefficient for Thin Films on Anisotropic Substrate. *J. Appl. Phys.* **2013**, *113*, 044111.

(27) Tsujiura, Y.; Kawabe, S.; Kurokawa, F.; Hida, H.; Kanno, I. Comparison of Effective Transverse Piezoelectric Coefficients $e_{31,f}$ of Pb(Zr, Ti)O_3 Thin Fi Lms between Direct and Converse Piezoelectric Effects. *Jpn. J. Appl. Phys.* **2015**, *54*, 1–8.

(28) Ye-Jing, D.; Xiao-Wen, Z.; Ke-Pi, C. Morphotropic Phase Boundary and Electrical Properties of $K_{1-x}Na_XNbO_3$ Lead-Free Ceramics. *Appl. Phys. Lett.* **2009**, *94*, 042905.

(29) Saito, T.; Wada, T.; Adachi, H.; Kanno, I. Pulsed Laser Deposition of High-Quality (K,Na)NbO_3 Thin Films on $SrTiO_3$ Substrate Using High-Density Ceramic Targets. *Japanese J. Appl. Physics,* **2004**, *43* (9 B), 6627–6631.

(30) Baker, D. W.; Thomas, P. A.; Zhang. N.; Glazer. A. M. Comprehensive Study of the Phase Diagram Of. *Appl. Phys. Lett.* **2009**, *95*, 091903.

(31) Ehara, Y.; Yasui, S.; Oikawa, T.; Shiraishi, T.; Oshima, N.; Yamada, T.; Imai, Y.; Sakata, O.; Hiroshi, F. Large Irreversible Non-180° Domain Switching after Poling Treatment in Pb(Zr, Ti)O_3 films. *Appl. Phys. Lett.* **2016**, *108*, 212901.

(32) Kovacova, V.; Vaxelaire, N.; Le Rhun, G.; Gergaud, P.; Schmitz-Kempen, T.; Defay, E. Correlation between Electric-Field-Induced Phase Transition and Piezoelectricity in Lead Zirconate Titanate Films. *Phys. Rev. B - Condens. Matter Mater. Phys.* **2014**, *90* (14), 140101.

(33) Kotera, I. K.; Hidetoshi, M.; Toshiyuki, M.; Wasa, K. Intrinsic Crystalline Structure of Epitaxial Pb(Zr, Ti)O_3 Thin Films. *J. Appl. Phys.* **2005**, *97*, 074101.

(34) Egerton, L.; Dillon, D. H. Piezoelectric and Dielectric Properties of Ceramics in the System Potassium-Sodium Niobate. *J. Am. Ceram. Soc.* **1959**, *42* (9), 438–442.

(35) Morimoto, K.; Kanno, I.; Wasa, K.; Kotera, H. High-Efficiency Piezoelectric Energy Harvesters of *c*-axis-Oriented Epitaxial PZT Films Transferred onto Stainless Steel Cantilevers. *Sensors Actuators, A Phys.* **2010**, *163* (1), 428–432.

(36) Shibata, K.; Suenaga, K.; Nomoto, A.; Mishima, T. Curie Temperature , Biaxial Elastic Modulus , and Thermal Expansion Coefficient of (K, Na)NbO_3 Piezoelectric Thin Films. *Jpn. J. Appl. Phys.* **2009**, *48* (121408), 1–5.

(37) Jo, W.; Daniels, J. E.; Jones, J. L.; Tan, X.; Thomas, P. A.; Damjanovic, D.; Rödel, J. Evolving Morphotropic Phase Boundary in Lead- Free ($Bi_{1/2}Na_{1/2}$)TiO_3 – $BaTiO_3$ Piezoceramics. *J. Appl. Phys.* **2011**, *109*, 014110.

FIGURES

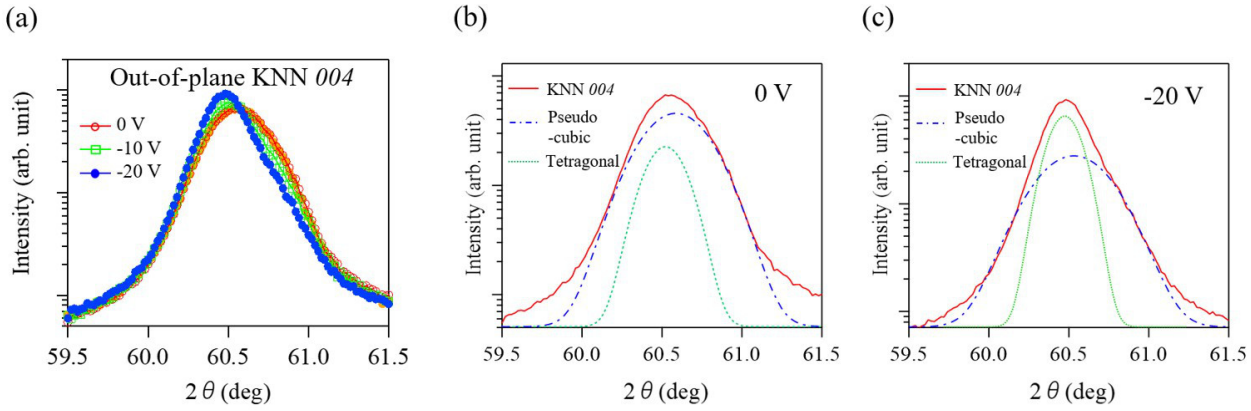

Figure 1. (a) Out-of-plane KNN peak patterns with various negative voltages. (b) KNN *004* peak pattern with fitting patterns without an applied voltage. (c) KNN *004* peak pattern with fitting patterns under an applied voltage of -20 V.

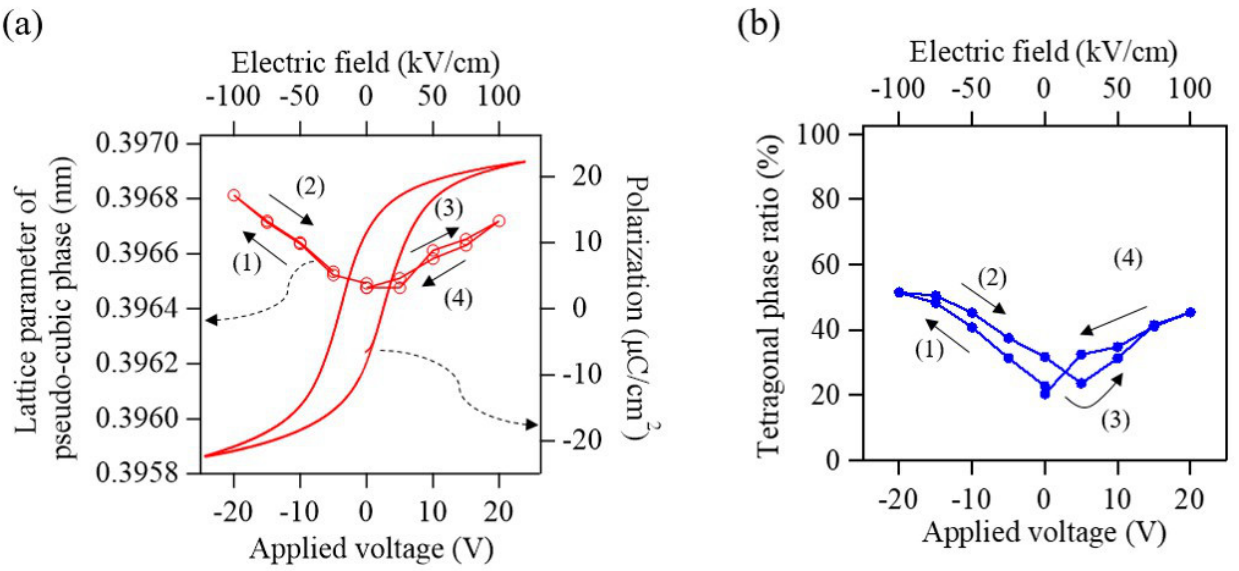

Figure 2. (a) Out-of-plane lattice parameter of pseudo-cubic phase as a function of applied voltage (electric field), superimposed with *P-E* hysteresis loop measured at 10 Hz. The number indicates the order of applied voltage. (b) Ratio variation of tetragonal phase as a function of applied voltage (electric field). The number indicates the order of applied voltage.

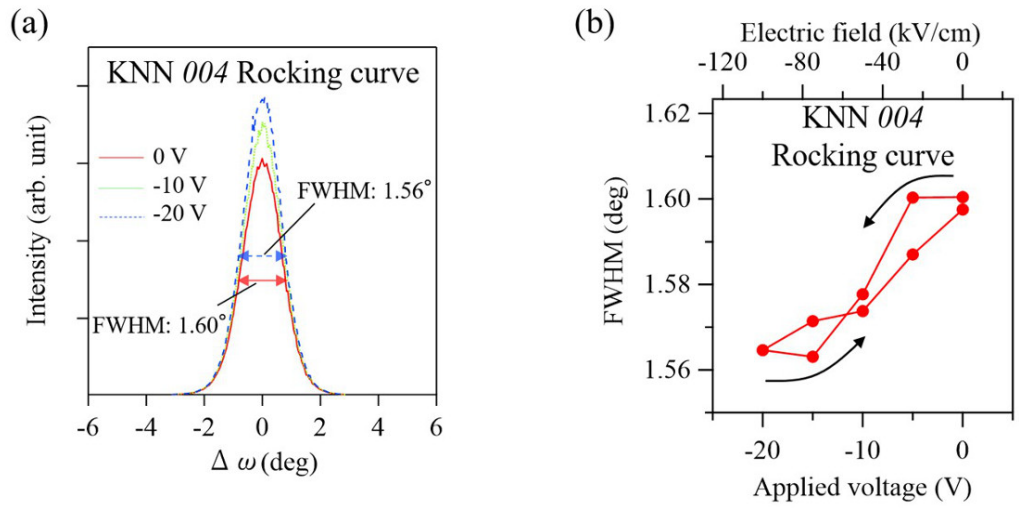

Figure 3. (a) *In situ* X-ray rocking curves of KNN *004* peaks with different voltages. The FWHM values are described for the 0 V and -20 V. (b) FWHM of rocking curves in the KNN *004* peaks as a function of applied voltage (electric field).

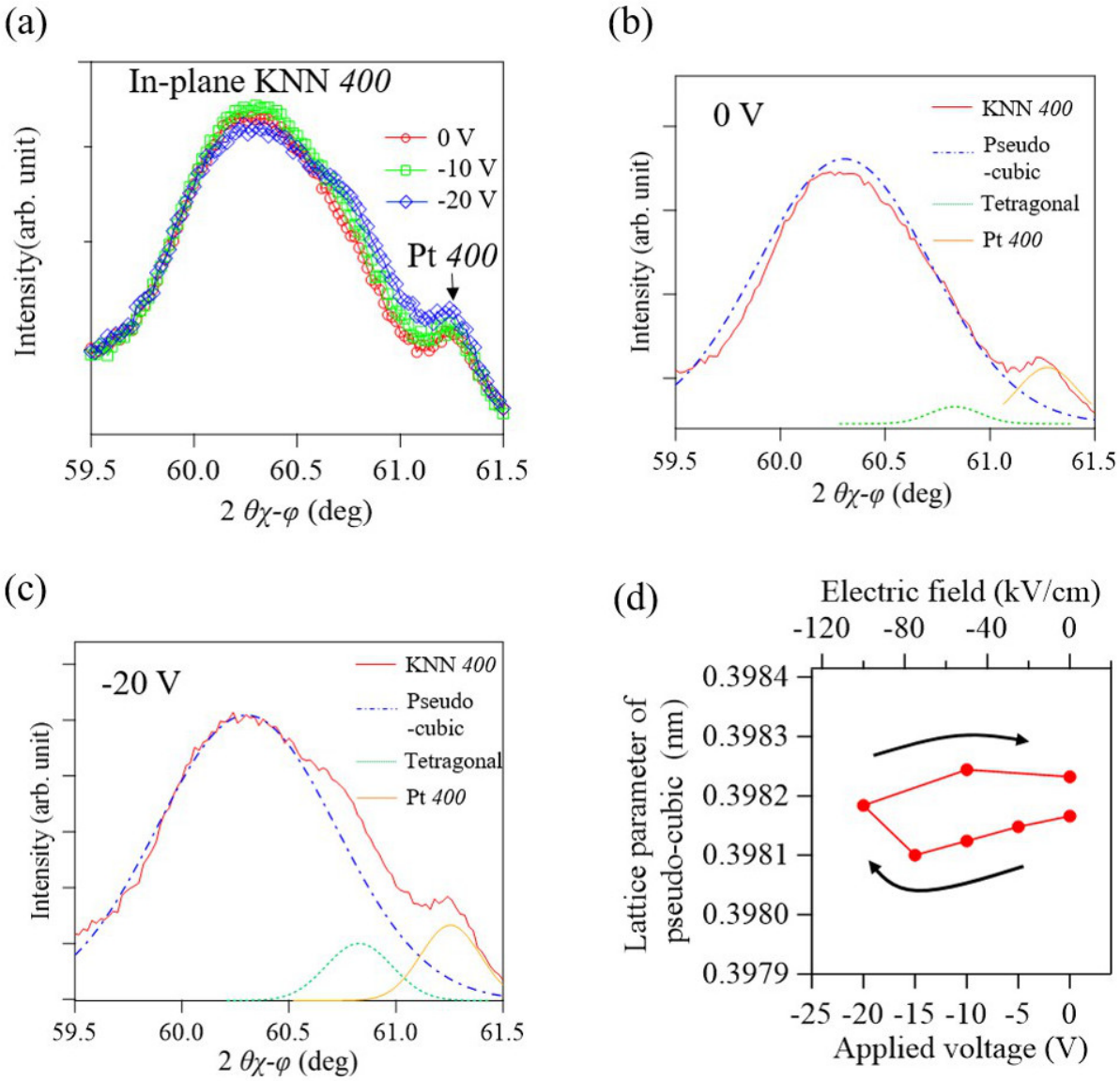

Figure 4. (a) In-plane XRD patterns of KNN peak with different negative voltages. (b) KNN *400* pattern with fitting curves without an applied voltage. (c) KNN *400* pattern with fitting curves under an applied voltage of -20 V. (d) In-plane lattice parameter of pseudo-cubic phase as a function of applied voltage (electric field).

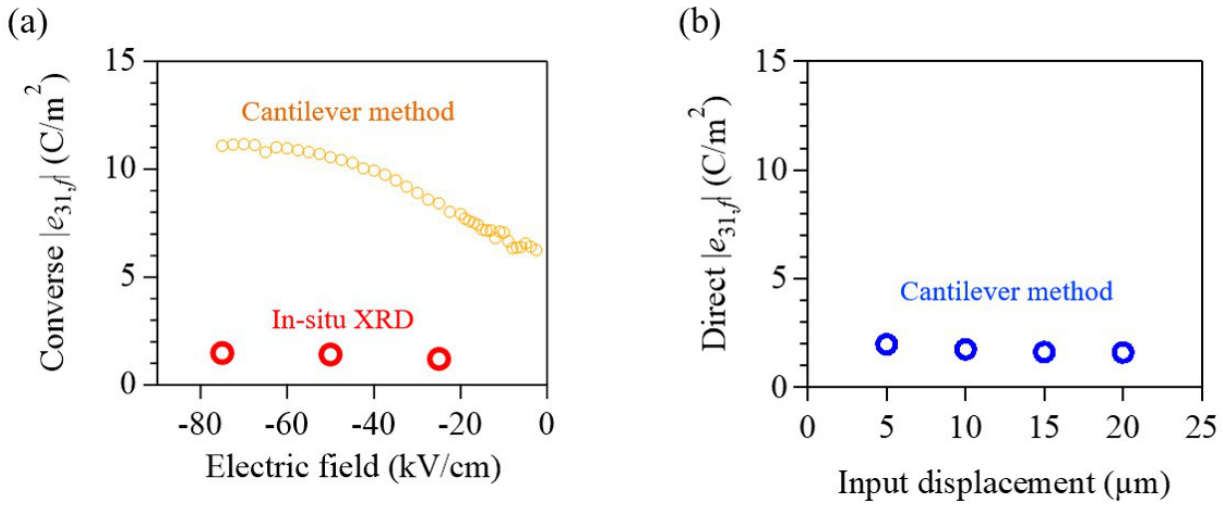

Figure 5. (a) Converse piezoelectric coefficients ($e_{31,f}$) as a function of negative electric field for the KNN thin film obtained from the cantilever method and the *in situ* XRD in-plane measurements. (b) Direct piezoelectric coefficient ($e_{31,f}$) as a function of input displacement by the cantilever method.